THESIS FOR THE DEGREE OF LICENTIATE OF ENGINEERING IN THERMO AND FLUID DYNAMICS

Unsteady Numerical Simulations of Flow around Heavy Vehicles, Trains and Passenger Cars

JAN ÖSTH

Department of Applied Mechanics
Division of Fluid Dynamics
CHALMERS UNIVERSITY OF TECHNOLOGY
Göteborg, Sweden 2012

Unsteady Numerical Simulations of Flow around Heavy Vehicles, Trains and Passenger Cars
JAN ÖSTH

Thesis for the degree of Licentiate of Engineering 2012:19
ISSN 1652-8565
Department of Applied Mechanics
Division of Fluid Dynamics
Chalmers University of Technology
SE-412 96 Göteborg
Sweden
Telephone: +46 (0)31-772 1000

Chalmers Reproservice
Göteborg, Sweden 2012

Unsteady Numerical Simulations of Flow around Heavy Vehicles, Trains and Passenger Cars
Thesis for the degree of Licentiate of Engineering in Thermo and fluid dynamics
JAN ÖSTH
Department of Applied Mechanics
Division of Fluid Dynamics
Chalmers University of Technology

Abstract

In this thesis several simulations have been carried out aimed at improving the knowledge of vehicle aerodynamics and improving the flow around vehicles with respect to the aerodynamic drag. Four flows around different simplified vehicle models have been considered. One model of a tractor-trailer, one passenger car model, one freight wagon model and one regional train model. The simplified tractor-trailer model consists of a front box representing a tractor and a rear box representing the trailer. The two boxes are separated by a gap width which is varied in the simulations. In the simulations on this geometry, the focus is on the flow in the gap between the tractor and the trailer and how this flow affects the global drag of the model. Large Eddy Simulation is used to simulate the flow around four variants of the model with different geometrical configurations. The behavior of the drag coefficient of the tractor-trailer model when varying the gap width and the shape of the front edges on the tractor is explained by identifying and analysing the large vortices around and in the the gap. The focus in the study on the passenger vehicle model is on the so-called A-pillar vortex. This is a swirling longitudinal vortex formed along the side windows on passenger vehicles due to the separation of the flow from the side edges of the front window and the engine hood. Flow control, both steady blowing and suction, from actuators located on the side of the front of the model is applied in the LES simulations. Steady blowing into the vortex causes expedited breakdown of the vortex, which in turn influence the pressure distribution on the side windows and the overall drag of the model. Steady suction causes the vortex to not form at all, thereby removing the vortex entirely. Simulations aimed at improving the knowledge of the flow around a generic freight wagon model using LES is also reported. The model is smoothed in comparison to a real container wagon, but the overall geometrical features such as wheels and underhood are included. The simulations of the flow around the regional train model is done using Partially Averaged Navier Stokes (PANS). PANS is a recently proposed hybrid turbulence model for engineering types of flow. The regional train model consists of a bluff body with a length to height/width ration of 7:1. The flow around this model poses several challenging flow situations to simulate such as separation from the leading curved front edges, an attached boundary layer flow and separation from the curved rear edges at the moderate Reynolds number of 400 000 based on the models' width. An open cavity is placed on the model at the base and the drag is thereby decreased by some 10%.

Keywords: fluid dynamics, vehicle aerodynamics, Large Eddy Simulation, bluff body flows, train aerodynamics, flow control, car aerodynamics, truck aerodynamics, flow physics, flow structures

Acknowledgements

I would firstly like to express my gratitude to my supervisor Prof. Siniša Krajnović for giving me this opportunity to deepen my knowledge in the very interesting field of CFD and vehicle aerodynamics and also for giving me great support during the project and providing a very stimulating research atmosphere with state-of-the-art resources. The PhD project is sponsored by the Swedish Traffic Administration, without the funding and the involvement of Peter Larsson this project would not be possible. I would also like to thank all my collegues at the division of Fluid Dynamics for creating a great working environment. Special thanks to my roommate Eysteinn who's constantly making sure my Linux installation is top notch and helping me with other computer related issues. I would like to thank Dr. Yutaka Samuka at Railway Technical Research Institute (RTRI) for sharing results and details of his experimental work. The lecture series in fundamental fluid dynamics given by the now retired Ass. Prof. Gunnar Johansson at the division during the winter and spring of 2011/2012 is greatly appreciated. The lectures gave a possibility for reflection by going back to the fundamentals which was very stimulating. Software licenses were provided by AVL List GMBH for which we are very grateful for. Special thanks goes also to Dr. Branislav Basara, Mr. Jürgen Schneider, Mr. Albert Van Der Meer and Dr. Wolfgang Schwarz at AVL for helping out with various issues regarding the software. Computations were performed at SNIC (Swedish National Infrastructure for Computing) at the Center for Scientific Computing at Chalmers (C3SE), Center for High Performance Computing at KTH (PDC) and National Supercomputer Center (NSC) at LiU. Least but not last I would like to thank my family for the support and my girlfriend Sigfrið Guðmundsdottír who has brought unprecedented joy to my life.

Thesis

This thesis consists of an extended summary and the following appended papers:

Paper A J. Östh and S. Krajnović. The flow around a simplified tractor-trailer model studied by Large Eddy Simulation. *Journal of Wind Engineering and Industrial Aerodynamics* 102 (2012), 36–47

Paper B S. Krajnović and J. Östh. LES Study of breakdown control of A-pillar vortex. *Int. J. Flow control* 2.4 (2010), 237–257

Paper C J. Östh and S. Krajnović. A study of the aerodynamics of a generic freight wagon with a container using Large Eddy Simulation. *Journal of Fluids and Structures* (2012), Under consideration

Paper D J. Östh and S. Krajnović. "Simulations of flow around a simplified train model with a drag reducing device using Partially Averaged Navier-Stokes". *Conference on Modelling Fluid Flow (CMFF'12), The 15th International Conference on Fluid Flow Technologies.* Budapest, Hungary, 4-7 September, 2012

Other publications related to the thesis by the author

Publication I J. Östh and S. Krajnović. "A LES Study of a Simplified Tractor-Trailer Model". *The Aerodynamics of Heavy Vehicles III: Trucks, Buses, and Trains.* Vol. 1. Potsdam, Germany, 2010

Publication II J. Östh and S. Krajnović. "Large Eddy Simulation of the Flow around one Single-Stacked Container Freight Wagon". *Proceedings of the First International Conference on Railway Technology: Research, Development and Maintenance.* Ed. by J. Pombo. Civil-Comp Press, Stirlingshire, Scotland, paper 162, 2012

Contents

Part I
Extended Summary

1 Introduction

Freight trains, regional trains and heavy vehicles are used all over the world to transport goods and peoples from one place to another. The modern world relies heavily on the functionality of these transport system amongst others. In the contemporary era more and more people are becoming aware of the fact that the energy resources available to the humans are not inexhaustible and that it therefore exists a constant need to optimize the utilization of the resources and to minimize the emissions of environmentally detrimental pollutants such as carbon dioxide. One of the major costs for transportation systems such as freight trains and heavy vehicles is the cost of the energy used to operate the systems. In the case of freight trains the main source of energy today in Sweden is electricity and for heavy vehicles fossil fuels. One contributor to the consumption of the energy put into a transportation system is the aerodynamic drag which is the concern of the work in this thesis. However, minimizing the aerodynamic drag is only one issue of many regarding aerodynamics of railway systems. This thesis is organized as follows. In this introduction some background on the energy consumption of trains, aerodynamic add-on devices and bluff body flows are given. This is followed by a brief introduction to turbulent flow and the simulations methods that have been used and a summary of the papers. Last, the four papers which is the foundation of this thesis are appended.

1.1 Aerodynamics issues regarding railway systems

During the construction of railway systems, including the design of the actual train occupying the railway, there are several serious issues emerging concerning the flow of the air around the train and the influence of the flow induced by the train on the sourrounding environments that need to be taken into consideration. One issue is the fuel consumption affected by the aerodynamic drag, other issues are slipstreams, crosswind effects, pressure waves radiating from train tunnels entries, ballast projection and aeroacousticly generated sound.

Slipstreams are the air being dragged along by the train, i.e., the boundary layer forming on the sides of the trains. This boundary layer is very strong and can cause serious accidents on people and materials on station platforms when train passes without stopping. Accidents related to slip streams from 1972 to 2005 in the United Kingdom (UK) are summarized in [7]. The train industry is subjected to regulations concerning the allowed slipstream velocities around trains. In the context of the European railway network, this is regulated by the Technical Specification of Interoperability (TSI) of rolling stock, directive 2008/57/EG, which specifies that a train operating at 200 km/h at 1.2 m above the platform and a distance 3 m from the center of the track should not exceed 15.5 m/s.

Slipstreams around high-speed trains have been investigated in experiments by Sterling et al. [8] and by numerical methods by Muld [9] and around freight trains by Hemida et al. [10].

The wind velocity perpendicular to the motion of the train during traction is called the crosswind. At large crosswind speeds the side and lift forces cause a turning moment around the leeward rail that can, in extreme cases, cause overturning of the train and derailment. Several serious accidents where trains have been overturned by the crosswind have occured. Crosswinds and the influence of geometric design parameters on trains on the vortices formed on the leeward side causing low pressure have been investigated by unsteady numerical methods in Hemida [11] and Krajnović et al. [12].

When trains enter tunnels, the air inside the tunnel is compressed and a pressure wave formed that travels with the speed of sound through the tunnel. When the wave hits the opposite entry, a part of the pressure wave is radiated to the surroundings and another part is reflected. The part that is radiated to the surrounding environment cause noise pollution and the part that is reflected back into the tunnel eventually hits the train travelling inside the tunnel and causes considerable discomfort for the passengers inside the train by both noise and vibrations. Travelling inside tunnels also increases the drag of the train significantly [13, 14, 15] and causes increased mechanical stress on the train. Tunnels, although necessary to overcome superfluous ascents, causes restrictions on the railway operations. This is espacially true for single-track tunnels where the ratio of the cross-sectional area of the train to the cross-sectional area of the tunnel is increased which leads to stronger pressure waves. Pressure waves and tunnel related aerodynamics are indeed a very important issue in the research on train aerodynamics [16, 17, 18]

Ballast projection is caused by the flow and pressure field underneath a train. The ballast consists of small gravel stones and rocks and as the train passes over them, the ballast stones can be dislodged and thrown against the undercarriage of the train. Flying stones phenomena underneath trains is referred to ballast flight. This can cause damage to the equipment underneath the train and the boogies. Underhood flow is studied experimentally by, for instance, Jönsson et al. [19].

In addition to noise caused by mechanical interaction of parts such as wheel/rail on the train, aeroacoustic noise is produced by the train when driving due to the air flowing around the train. The source of the noise is flow separation caused by either the detachment of the boundary layer on the train or by vortex shedding from protruding structural elements on the train. The strengh of the noise is proportional to the speed of the train by a power of 6-8 [20]. Thus, the noise alleviation is of immense practical importance when train speed increases. Protruding objects on the train is the main source of aeroacoustic sound. For instance, the pantograph on the roof of the train which usually have a cylindrical shape can cause a monotone noise due to the vortex shedding behind it which propagates and pollutes the environment far away from the railway. All roughnesses on the train contributes to the aeroacoustic noise and also the nose shape of the train has a large impact. It is desirable to have a fore-body configuration with a long nose to

reduce the aerodynamic noises. [16]

1.2 Energy consumption of trains and aerodynamic drag

The sum of the resistive forces acting on trains in the direction of travel is usually expressed as a second order polynomial [21, 16, 22, 23]:

$$F = A + B \times V + C \times V^2 \tag{1.1}$$

It is assumed in Eq. 1.1 that the train does not accelerate or decelerate, that it travels on flat ground and that the railway is straight. Otherwise, terms for the forces needed to overcome the resistance of acceleration, the gravitational force and mechanical curving resistance must be included in Eq. 1.1. The term A on the right hand side contains mechanical resistances that are constant with respect to the speed of train, V, but whose magnitude is dependent on the number of axles, axle loads, track type and the length of the train. The second term contains mechanical resistances coming from moving parts on the train and vary with the length of the train and are linearly proportional to the speed. The last term contains the aerodynamic resistance of the train, which is proportional to the square of the speed. The values of the coefficients in Eq. 1.1 are highly dependent on each specific type of train under consideration and must be determined individually for each specific train [24, 23, 22]. Empirical equations that can be used to estimate the resistance of a general train configuration have been developed. See [22] for a review of empirical equations used to estimate resistances of trains. A freight train normally consists of a large amount of wagons of different sizes, shapes and purposes. For a freight train, the coefficient C in Eq. 1.1 is the sum of the contribution to the aerodynamic drag from the locomotive and all wagons in the train. The size of the contribution to C of each wagon depends on the position of the wagon in the train [25] as well as on the spacing between the wagons [26, 27].

Figure 1.1 shows the drag coefficient of a closed top gondola-type freight wagon depending on the position in the train. Results are shown for 0, 5 and 10 degrees of yaw angle. It is seen in the figure that, after the initial 3-4 wagons, the drag coefficient will reach some steady value that is some 20-50% less than the drag coefficient of the second wagon. The majority of all the wagons in a freight train will experience an aerodynamic drag force slightly lower than that experienced by the first wagon in the train. The contribution to the total drag of the entire train from the locomotive will in turn be higher than the drag of the second wagon due to the stagnation pressure of the air on the front of the locomotive. A study reported in [28] suggests that the drag coefficient of the locomotive is in the order of 4 times of the drag coefficient of the first wagon (thus the wagon in position 2 in Fig. 1.1). The total drag coefficient of a freight train consisting of a locomotive and 70 wagons of various sizes and shapes are estimated in [27] to be around 18.

A typical regional train concists of 3-4 units and its length is around 60-70 m. The

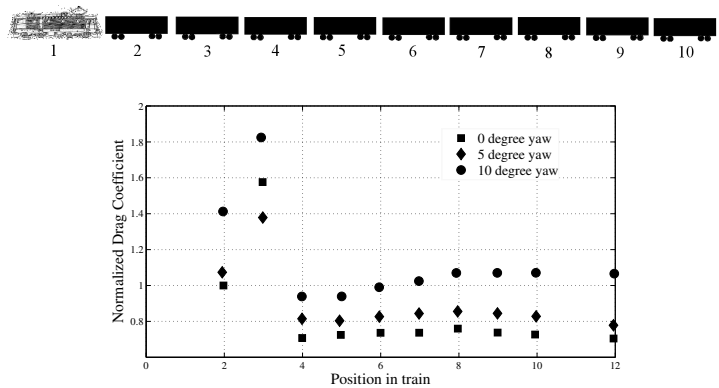

Figure 1.1: *The top figure shows an arbitrary container freight train with a locomotive and 10 single stack wagons.The bottom figure shows the drag coefficient (y-axis) for a closed top gondola-type freight wagon depending on the position in the train (x-axis). All the values are normalized with the value of the drag coefficient of the wagon in the second position at zero yaw angle. The results are redrawn from the full-scale experimental study reported in [25].*

operation of regional trains are characterized by short driving cycles ($\approx 1\,h$) where the trains make several stops during the cycle and the maximum speed is below 150-160 km/h. Due to the stops, the part of the journey that the train has maximum speed is considerable shorter than the actual journey. This diminishes the relative influence of the aerodynamic drag on the total energy consumption.

One train used for regional traffic in Sweden is shown in Fig. 1.2. This is the Bombarbier Contessa train. As can be seen by a layman, the shape of the train is not optimal from an aerodynamic drag minimizing point of view. This is true in general for trains that are used for regional traffic. Less effort has been invested by the manufacturers on reducing the aerodynamic drag, due to it's relative less importance on the fuel consumption in comparison to high speed trains. The energy put into the railway system are consumed by different resistances. The energy demand for a general electric powered train is shown in Fig. 1.3.

The losses of the energy in the system are divided into the following components:

- E_{VI}: infrastructure losses
- E_{Vd}: driving losses
- E_{Vb}: braking losses
- E_{BR}: brake resistor losses

Figure 1.2: *Bombardier Contessa train used in Sweden for regional traffic.*

As is seen in Fig. 1.3, already some 20% of the energy provided by the substation is lost in the electric infrastructure on the way to the train. The driving losses E_{Vd} corresponds to some 55% of the energy demand. This energy is dissipated to heat in the environment by the aerodynamic drag and mechanical resistances. This part cannot be regenerated, while some part of the energy that is converted to kinetic energy can be regenerated by the braking system.

The driving losses E_{Vd} are caused by the resistive forces acting on the train expressed in Eq. 1.1. In the estimate done in Orellano and Sperling [29] on a generic regional train on a typical driving cycle, a decrease in the aerodynamic drag coefficient of the train by 30% would lead to a 13 % decrease in the traction energy. There thus exists some potential for energy savings by improvement of the aerodynamics of regional trains. The total drag of a regional train comes from different parts on the train, as for freight trains. An estimate of the contribution to the drag and potential for reduction is shown in Fig. 1.4. The pressure drag from the head and the tail of the train accounts for some 30% of the total. Other main sources are the various protroduing objects and the skin friction.

1.3 Bluff body flows

The term bluff body flow refers to flows over bodies which is strongly influenced by flow separation due to the shape of the body and where the pressure forces are dominant over frictional forces. With flow separation means that the fluid breaks loose from the surface of a body and a region of reversed flow arises. This creates regions with large eddies that contribute to lower pressure. For vehicle the drag is often increased by flow separation from the front or the rear. Bluff bodies are often characterised by separation at the front edge, however, the separation may also be at the rear end. All flows over road vehicles

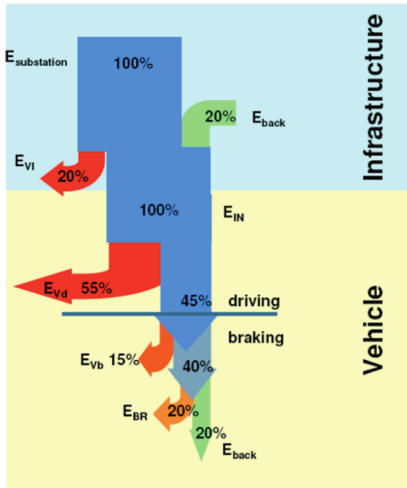

Figure 1.3: *Traction energy demand distribution for railway system. The figure is taken from Orellano and Sperling [29]*

and trains fall into the category of bluff body flows. Even though modern vehicles most often are designed in a streamlined manner, separation takes place on the rear, but also at inter-car gaps, underbody, roof etc. The aerodynamic drag consists of two parts, the first is the pressure drag component and the second is the skin friction due to the momentum transfer from the fluid molecules to the surface of the body in near wall region. For road vehicles, the skin friction is negligible and of much smaller order than the pressure drag which is due to the difference in pressure of the front and base of the body. However, the skin friction plays a crucial role in the aerodynamics of high speed trains where it is in the same order as the pressure drag.

1.4 Aerodynamic add-on devices

Aerodynamic add-on devices are used extensively on modern tractor-trailers. With the advent of the oil crisis in the 1970's, a high interest in improving the energy efficiency of heavy vehicles emerged. This led to extensive research during the 1970s and 80s in the aerodynamics of trucks [31, 32]. The most obvious improvement of the design that lead to a substantial reduction in the aerodynamic drag of trucks was aerodynamic shaping of the front. Busses and trucks have naturally a rectangular shape due to loading capacity and functionality. They can be considered as bluff bodies. A buss might be represented by one rectangular block and a truck by two, one representing the tractor and one the trailer. One important parameter in both these cases is the rounding of the front edges. The drag of a rectangular block depends on the rounding of the front edges, as shown in Fig. 1.5.

It is seen in the figure that for no radius the drag is more than 50% higher than

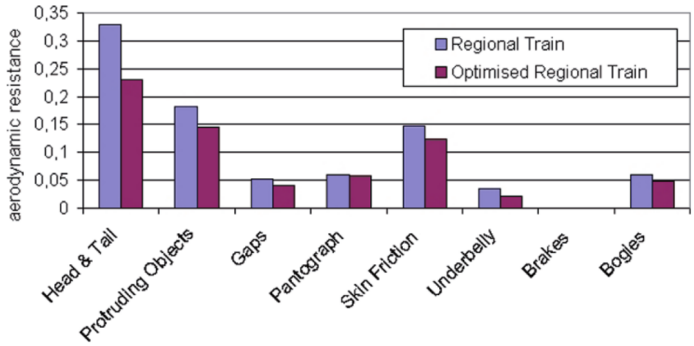

Figure 1.4: *Estimated potential for reducing the drag of a regional train. The figure is taken from Orellano and Sperling [29]*

for larger radiuses. This is due to the accelerating air over the curvature part. The accelerating air impose a low pressure on the curved surface. Since the curvature is exposed to the streamwise direction, the low pressure will contribute to a decrease the the global drag coefficient. If the radius of the curvature is increased, so is the exposed area to the streamwise direction and the global drag force is thereby decreased. This contributes to the significant reduction of the drag coefficient as the radius increases as seen in Fig. 1.5. The distribution of the sources and their magnitues to the total drag coefficient of a schematic tractor-trailer is seen in Fig. 1.6. The values in the figure should be taken as an indication of how the drag is distributed on a tractor-trailer. The overall drag coefficient is 0.7 of which 0.2 comes from the front, 0.2 from the gap between the tractor and the trailer, 0.2 from the wake behind the trailer and 0.1 from the wheels. Variuos devices are used on modern tractor-trailers to decrease the drag from the different areas. In the gap it is standard to use gap fairings, cab extendors or air deflectors which reduce the effective gap width and thereby contributes to a streamlining of the body. In general, the smaller the gap width is the better from a drag point of view. However, zero gap is hard to achieve due to restrictions in the maneuverability that would be caused by such a design. Several techniques have been tried extensively to reduce the drag in the wake of the tractor-trailer with various success. Examples of such techniques are flow control using shaped actuators [34], cavities [35, 36] and boat tails [37].

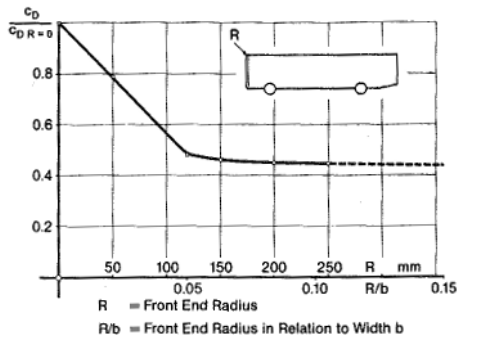

Fig. 9.56 Influence of front radii on drag.

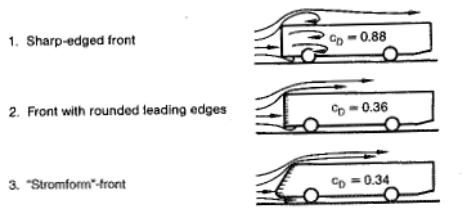

Figure 1.5: *Relation between shape of vehicle front and drag coefficient. The figure is taken from Hucho [30].*

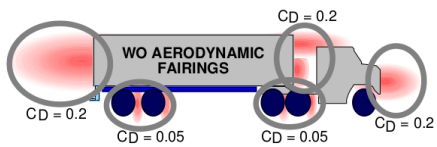

Figure 1.6: *Graphic depicting the distribution of aerodynamic drag for a heavy vehicle tractor-trailer truck. The figure is taken from Wood and Bauer [33].*

1.5 Project outline

This thesis is part of a 5-year PhD project where the overall objective is to investigate how aerodynamic drag on freight and regional trains can be reduced by the use of so called aerodynamic add-on devices. Add-on devices such as deflectors, side-skirts and even vortex generators are used extensively on heavy vehicles and passenger vehicles successfully reducing the aerodynamic drag and thereby the energy consumption of these vehicles. The goal of the PhD thesis is to investigate how similar devices can be used on trains. The focus in the PhD project is on freight and regional train due to the fact that high-speed trains already have a rather efficient design from an aerodynamic drag minimizaing point of view, while freight and regional trains generally is not designed to minimize the aerodynamic drag and therefore a larger potential exists to reduce the drag of existing trains by utilization of aerodynamic add-on devices.

2 Techniques to simulate unsteady turbulent flows

Almost all flows, regardless of the working fluids (gases and liquids), encountered in engineering and daily life are turbulent. There exists no exact definition of what turbulence really is, but turbulent flows do have certain recognizable characteristics. They are e.g. intrinsically complex, nonlinear and there is a large spread of the time scales as well as the spatial scales in the flow. The swirling motions observed in daily life such as flowing water in rivers, the pillars of air from plumes, the air around vehicles, are all examples of turbulent flows where the chaotic behavior of turbulent flow is visible to our eyes by the natural flow visualisation. Another characteristics of turbulent flows are irregularity and randomness. Turbulence is an omnipresent phenomenon whether it's in the processing of fluids and gases in pumps, compressors, pipes, the flow around vehicles such as airplanes, automobiles, trains, ships, or the mixing of air and fuel in engines and air and reactants in chemical reactors. Thus, there's no way to avoid the influence of turbulence nor to ignore it when constructing and studying such systems. The scientific study of turbulence takes different approaches, such as the statistical approach enabled by, for instance, the Reynolds decomposition. That is, to ignore the details of the instantaneous flow and instead regard the flow as a superposition of a statistically well-defined mean part and a fluctuating part. This allows for the use of statistical and probabilistic methods to study the nature of turbulence. Another common approach is the phenomenlogical approach where the actual geometrical features of the instantaneous turbulence are characterized and universal coherent and incoherent structures are identified and interpreted, thus, in some sense trying to find order and coherence in the apperent randomness in the chaotic flow. It is generally accepted that the Navier-Stokes equations (NSE) mathematically model the flow of fluids at a macroscopic level and accurately describes what is observed in nature, even though no mathematically unique and smooth (continuously differentiable) solutions at high Reynolds numbers have been proven to exist so far [38]. NSE for an incompressible, single-phase flow, with dynamic viscocity μ and density ρ read:

$$\frac{\partial u_i}{\partial x_i} = 0. \tag{2.1}$$

$$\frac{\partial u_i}{\partial t} + u_j \frac{\partial u_i}{\partial x_j} = -\frac{1}{\rho}\frac{\partial p}{\partial x_i} + \nu \frac{\partial^2 u_i}{\partial x_j \partial x_j} + f_i. \tag{2.2}$$

Equation 2.1 being the continuity equation expressing the conservation of mass and Eq. 2.2 is the momentum equations expressing conservation of momentum. $u_{i=x,y,z}$ are the three components in the velocity vector in a Cartesian coordinate system, $\nu = \mu/\rho$ is the kinematic viscocity of the fluid and f_i possible body forces.

In vehicle aerodynamics, the single most important parameter characterizing any flow around vehicles is the large scale Reynolds number. It is usually expressed as:

$$Re = \frac{\mathcal{U}\mathcal{L}}{\nu} \tag{2.3}$$

Where the velocity scale $\mathcal{U}$ is taken to be the free-stream velocity and the length scale $\mathcal{L}$ is usually taken as the height or the length of the vehicle being studied. The Reynolds number is an appreciation of the ratio of the magnitude of the convective term (second term on l.h.s. in Eq. 2.2) to the magnitude of viscous term (second term on r.h.s. in Eq. (2.2). The convective term is a nonlinear term which is the source of the irregularity, randomness and chaotic behavior of turbulent flow. Thus, the higher the Reynolds number is in a flow, the more pronounced is the influence of turbulence. For a sufficiently low Reynolds number, the flow is laminar. This is due to the viscous forces being large enough to be able to dampen out any non-regular fluctuation in the flow. As the Reynolds number increases for a given flow situation, the flow undergoes a transition from laminar state to turbulent state

For passenger cars the Reynolds number on roads during normal cruising speed is in the order of $10^6 - 10^7$ and for trains they are in the order of $10^7 - 10^8$. The scales in turbulent flows range from vortices and swirling motion of the size of $\mathcal{L}$ down to the smallest scales in the flow, the so called Kolmogorov scales, which are smaller than millimeters for vehicle flows. The large scales carry most of the kinetic energy of the fluid, while the dissipation of the kinetic energy of the fluid to internal energy (heat) takes place at the smallest scales. This is illustrated in Fig. 2.1, where l_0 is the characteristic size of the anisotropic energy-carrying scales, l_{EI} is a limit where the energy-carrying scales can be considered to be isotropic and, according to Kolmogorov theory, the statistics is universal. This range is called the *universal equilibrium range* and consists of two subranges, the *inertial subrange* and the *dissipation range.*

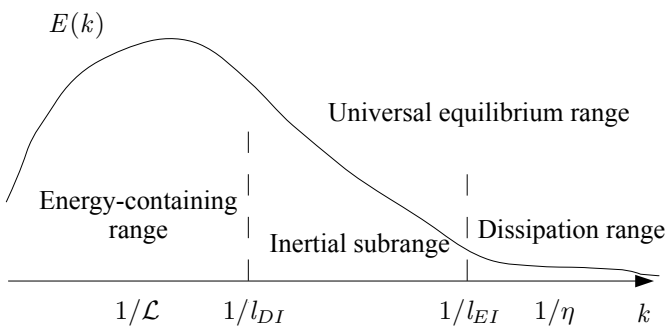

Figure 2.1: *Idealized picture showing the energy content in a turbulent flow as a function of the wave number k (logaritmic scale).*

According to Kolmogorov's second similarity hypothesis the motions in the inertial subrange are determined primarily by inertial effects, thus viscous effects being negligible

and the motion in the dissipation range the motions are governed by strong viscous effects and are thus responsible for essentially all of the energy-dissipation. The process that kinetic energy is transferred from the large, energy-carrying scales through the inertial subrange to the dissipation scales is called the *Cascade-process*.

When numerically solving Eqs. 2.1 and 2.2 all scales of motion need to be resolved in order to obtain an accurate estimation of the real flow. That is, all the scales from the large scales down to the smallest, dissipative scales should be resolved. This approach is called Direct Numerical Simulation (DNS), and due to the very small character of the dissipative scales, the computational cost for such simulations are unfeasible for any engineering type of flow. Thus, some kind of model is needed to get an approximation of the full DNS solution of the flow. By using the Reynolds decomposition that divides the flow into a mean part and a fluctuating part, $u_i = \langle U_i \rangle + u'$, and inserting this into the governing equations, the Reynolds Averaged Navier Stokes equations are obtained. This approach is the basis for steady state engineering turbulence models such as the $k - \epsilon$ model and various Reynolds Stress Models. This method presupposes a large separation of the turbulent fluctuating scales and the energy-carrying scales (the "mean" flow). As this is not the case in most kinds of bluff body flows, but the scales are continously distributed from the large scales to the smallest, it is not correct to employ this type of methods to vehicle aerodynamics and expect reliable results. In this thesis, the method of Large Eddy Simulation (LES) has been used as well an recently developed unsteady method called Partially Averaged Navier Stokes (PANS), although both methods are unsteady they are fundamentally different. In the coming sections LES, being a rather well-known method, will only briefly be described, while a more elaborate outline of PANS is provided.

2.1 LES

Large Eddy Simulation (LES) is a collective term used to denote certain methods which are all based on the same conceptual idea that the large, energy-carrying scales are resolved directly, while the small scales (the universal scales according to Kolmogorov theory) are not resolved, but the influence of them is modelled. The physical motivation behind this idea is the assumption of the universality of the small scales described briefly in the former section. An implicit prerequisite for the idea of LES to work is that the large scales are resolved down to the inertial subrange where the scales presumably become isotropic. In practise, this is done by careful selection of the applied numerical grid when carrying out the simulation of the flow. There are many ways in which LES can be done mathematically, such as the spectral method which is based on the spectral NSE (the Fourier transformed Eqs. 2.2), implicit LES where the numerical dissipation from the discretization schemes is used to balance the equations and thereby resolve only the large scales, and explicit sub-grid models where an explicit mathematical model is used to model the influence of the smallest scales on the resolved ones after a spatial filter has been applied to the NSE. The latter method is the one used in this thesis. No comprehensive investigation or complete review of methods are provided herein, the reader is referred to e.g. [39, 40] for a detailed theoretical analysis of LES, different sub-grid models and its

mathematical foundations. Herein the specific sub-grid model (Standard Smagorinsky Model) that has been used in this thesis will be described briefly. The governing equations of LES (the filtered Navier-Stokes) are obtained by applying a spatial filter on Eqs. 2.1 and 2.2. The general filter operation applied on an arbitrary function $f = f(\mathbb{x}, t)$ (denoted by "overbar") is defined by:

$$\bar{f}(\mathbb{x}, t) = \iiint G(\mathbb{r}, \mathbb{x}) f(\mathbb{x} - \mathbb{r}, t) d\mathbb{r}, \tag{2.4}$$

the filter function G must satisfy the normalization condition

$$\iiint G(\mathbb{r}, \mathbb{x}) d\mathbb{r} = 1. \tag{2.5}$$

The LES concept is based on the decomposition of the velocity field into the resolved motion (filtered velocities) and the small-scale motion that are filtered away a priori (sometimes denoted sub-grid scales or residual field), i.e.:

$$\mathbb{u}(\mathbb{x}, t) = \bar{\mathbb{u}}(\mathbb{x}, t) + \mathbb{u}''(\mathbb{x}, t) \tag{2.6}$$

This should not be confused with the Reynolds decomposition mentioned in the beginning of the chapter. The most important factor being that the filtered velocity field, $\bar{\mathbb{u}}(\mathbb{x}, t)$, is a random field while the ensembled averaged velocity is not. The residual field, $\mathbb{u}''(\mathbb{x}, t)$, is never obtained explicitly in any LES simulation, and can only be obtained if a fully resolved DNS simulation has previously been conducted with exactly the same conditions. By applying the filter operation defined by Eq. 2.4 on the incompressible Navier-Stokes equations, the filtered NSE are obtained:

$$\frac{\partial \bar{u}_i}{\partial x_i} = 0. \tag{2.7}$$

$$\frac{\partial \bar{u}_i}{\partial t} + \bar{u}_j \frac{\partial \bar{u}_i}{\partial x_j} = -\frac{1}{\rho} \frac{\partial \bar{p}}{\partial x_i} + \nu \frac{\partial^2 \bar{u}_i}{\partial x_j \partial x_j} - \frac{\tau_{ij}^R}{\partial x_j}, \tag{2.8}$$

where the force term has been dropped for convenience. The last term is the residual stress tensor, $\tau_{ij}^R = \overline{u_i u_j} - \bar{u}_i \bar{u}_j$. This part is split into an anisotropic part and an isotropic part: $\tau_{ij}^R = \tilde{\tau}_{ij}^r + \frac{1}{3} \tau_{kk}^R \delta_{ij}$. The isotropic residual stress tensor is included in the filtered pressure, $\bar{p}$, and Eq. 2.8 is written as:

$$\frac{\partial \bar{u}_i}{\partial t} + \bar{u}_j \frac{\partial \bar{u}_i}{\partial x_j} = -\frac{1}{\rho} \frac{\partial \bar{p}}{\partial x_i} + \nu \frac{\partial^2 \bar{u}_i}{\partial x_j \partial x_j} - \frac{\tilde{\tau}_{ij}^r}{\partial x_j}, \tag{2.9}$$

The model used to close the anisotropic residual stress tensor $\tilde{t}_{ij}^r$ used in Paper A, B and C in this thesis is the Smagorinsky model first proposed by Smagorinsky [41]. The residual stress tensor is modeled by an eddy-viscosity assumption:

$$\tau_{ij}^r = -2\nu_{sgs} \bar{S}_{ij}. \tag{2.10}$$

That is, the unresolved scales are said to be proportional to an artificial "eddy" viscosity and the rate-of-strain tensor of the filtered velocities $\bar{S}_{ij} = \frac{1}{2}(\frac{\partial \bar{u}_i}{\partial x_j} + \frac{\partial \bar{u}_j}{\partial x_i})$. The eddy viscosity, ν_{sgs}, is then modelled by an "mixing-length" hypothesis:

$$\nu_{sgs} = l^2 \bar{S} = (C_s \Delta f)^2 \bar{S}. \tag{2.11}$$

The eddy viscosity is taken to be proportional to the square of a characteristic length scale of the unresolved scales and the magnitude of the rate-of-strain tensor. The length scale is taken to be the product of the filter width Δ and the Smagorinsky constant C_S. In this work, the filter width is taken to be the local grid size, $\Delta = (\Delta x \cdot \Delta y \cdot \Delta z)^{1/3}$ and the Smagorinsky constant is taken to be $C_S = 0.1$ which is a value that has been used in numerous investigations of vehicle aerodynamics bluff body flows [42, 11, 43, 44]. It should be noted that, for complex geometries using non-equidistant computational grids as in the present thesis, a commutation error is introduced since the formulation of filtered equations (Eqs. 2.7 and 2.8) assumes that the filtering operation and spatial derivation commute. This is however not true on non-equidistant grids. The commutation error introduced is of the same order as the truncation error of a second-order linear interpolation scheme [45]. The function f is the Van Driest damping function:

$$f = 1 - e^{n^+/25} \tag{2.12}$$

which is added to make ν_{sgs} vanish at the wall. Although the Smagorinsky model is the simplest sub-grid stress model, the method can be viewed from an mathematical point of view as adding a non-linear viscosity to the fluid since the filtering is never applied explicitly in the formulation of the method but it is implied implicitly. It turns out that the Smagorinsky model actually provides a regularization of the NSE that transforms the (possibly ill-posed) NSE into a well-posed set of partial differential equations, see e.g. Guermond et al. [46].

2.2 PANS

In paper D in this thesis, the unsteady flow around a simplified train model is simulated using the recently developed unsteady method Partially Averaged Navier Stokes (PANS). The PANS method was proposed by Girimaji [47] as a bridging/hybrid approach of turbulence modeling for engineering types of flows developed from the first principles. The objective when deriving the method was to improve the inherent modeling defects of the Unsteady Reynolds Averaged Navier-Stokes approach (URANS). In an URANS simulation, the RANS equations are solved in a time-accurate fashion on a grid with a relatively good spatial resolution and with low turbulence kinetic energy and thus low eddy viscosity on the inlet [48]. The intention with URANS is to resolve smaller unsteady scales of motion than those that are averaged away in steady RANS simulations. The URANS fails however, because the eddy viscosity becomes to large and supresses the temporal and spatial fluctuations that could have been supported by the grid and temporal resolution. The failure of URANS is due to the ratio of produced turbulence kinetic energy to dissipation is too high (un-physical) which disables URANS to resolve

the fluctuating motions [49]. PANS offers a method to prevent the eddy viscosity to blow up by modifying the coefficients of the parent RANS model in a physical correct manner according to the local resolution of the flow field in time and space and the amount of resolved and unresolved fluctuations. The method thus seeks to maximize the amount of fluctuations that are resolved directly and which can be handled on a given grid and flow situation. To derive the PANS method, a model equation for the unresolved (sub-filter) kinetic energy k_u was derived from the equation of the generalized central moments ([50]):

$$\begin{aligned}\frac{\partial \tau(u_i,u_j)}{\partial t}+\frac{\partial \tau(u_i,u_j)\bar{u}_k}{\partial x_k} &= -\frac{\partial}{\partial x_k}\{\tau(u_i,u_j,u_k)+\\ &\tau(p,u_i)\delta_{jk}+\tau(p,u_j)\delta_{ik}-\nu\frac{\tau(u_i,u_j)}{\partial x_k}\}\\ &+2\tau(p,S_{ij})-2\nu\tau(\frac{\partial u_i}{\partial x_k},\frac{\partial u_j}{\partial x_k}\\ &-\tau(u_i,u_k)\frac{\partial \bar{u}_j}{\partial x_k}-\tau(u_j,u_k)\frac{\partial \bar{u}_i}{\partial x_k}.. \end{aligned} \tag{2.13}$$

Here, u_i is the instantaneous unfiltered / unaveraged instantaneous velocity variables and $\bar{u}_i = \langle u_i \rangle$ is the filtered /averaged velocities. The function $\tau(f,g) = \langle fg \rangle - \langle f \rangle \langle g \rangle$ is the generalized central moment of the functions f and g and the angular brackets $\langle . \rangle$ corresponds to a filter that is constant preserving and commuting with both spatial and temporal differentiation. In case of LES, this filter is the spatial filted defined in Eq. 2.4. Equation 2.13 is obtained by manipulation of NSE. The kinetic energy of the unresolved scales is the trace of the central moment, $k_u = \frac{1}{2}\tau(u_k,u_k)$. An equation for the dissipation ϵ_u of the unresolved scales was constructed phenomenologically in the derivation of PANS. To make PANS sensitive of the resolved scales of motion in the flow, the decisive parameters $f_k = k_u/k$ and $f_\epsilon = \epsilon_u/\epsilon$ (ratio of unresolved kinetic energy/dissipation to total kinetic energy/dissipation) was introduced into the derivation of the governing equations. How this was done will be explained in the coming paragraphs. It is important to stress that PANS is neither a RANS model, nor is it a LES model or a hybrid LES/RANS model. It is a unique method based on derivations from the first principles, but having some features common with both RANS and LES inherent to it.

The original PANS ([47]) was derived using the standard $k-\epsilon$ RANS model as parent model. This model will be denoted PANS $k-\epsilon$ hereafter. The PANS $k-\epsilon$ method was tested on the flow around a square and circular cylinder in [51, 52], respectively. As noted in Girimaji [47], the quality of the results in a simulation with PANS will be inherently dependent on the quality of the parent RANS model. Soon enough, a version of PANS based on the $k-\omega$ RANS model was introduced by Lakshmipathy and Girimaji [53]. In Girimaji et al. [49] the ratio of produced unresolved kinetic energy to dissipation in PANS was compared both theoretically and computationally with URANS and DES. It was found that PANS resolved more unsteady vortical structures than the two latter methods for the given cases being studied and the employed grids, and PANS showed better agreement with experimental data as well. In [54] PANS was combined with a Low Reynolds Number (LRN) $k-\epsilon$ RANS model in order to correct

the inherent inappropriate behavior of the PANS $k-\epsilon$ model near the wall due to the deficits in the standard RANS $k-\epsilon$ model. The performance of PANS LRN in standard cases such as decaying grid turbulence, turbulent channel flow and the periodic hill flow was investigated with promising results. It was also found that PANS LRN give better results than the Dynamical Smagorinsky LES model at a reduced CPU time for these cases.

Another method to enhance the performance of the k-ϵ RANS model in the near wall region is the four equation $k-\epsilon-\overline{v^2}-f$ RANS method proposed in [55] and later reformulated to the $k-\epsilon-\zeta-f$ model by Hanjalić et al. [56]. In these so called elliptic-relaxation based eddy viscosity models, two additional (to k and ϵ) model equations are derived and solved for the wall-normal velocity $\overline{v^2}$ scale and the relaxation function f. This enables RANS to take into account the inviscid wall blocking effect while incorporating low Reynolds number effects in the viscous and buffer sublayers of the turbulent boundary layer. The PANS method based on RANS $k-\epsilon-\zeta-f$ was initially developed by Basara et al. [57] and further motivated by Basara et al. [58] where it was validated against channel flow and the complex flow around a finite cylinder [59]. The PANS $\zeta-f$ version was used in Krajnović et al. [60] to simulate the complex and relatively high Reynolds number unsteady flow around the Rudimentary Landing Gear [61, 62] with very promising results.

An overview of the derivation and the development leading up to the PANS model used in this thesis (PANS $\zeta-f$) follows here. The starting point is the partially filtered Navier-Stokes equations:

$$\frac{\partial \bar{u}_i}{\partial t}+\bar{u}_j\frac{\partial \bar{u}_i}{\partial x_j}=-\frac{1}{\rho}\frac{\partial p_F}{\partial x_i}+\frac{\partial}{\partial x_j}(\nu\frac{\partial \bar{u}_i}{\partial x_j}-\tau(u_i,u_j)) \tag{2.14}$$

$$\bar{u}_i=\langle u_i\rangle;\quad p_F=\langle p\rangle \tag{2.15}$$

$$\tau(u_i,u_j)-\frac{2}{3}k_u\delta_{ij}=-2\nu_u\bar{S}_{ij} \tag{2.16}$$

Where $u_i,\ p$ are the instantaneous unfiltered flow variables and $\bar{u}_i,\ p_F$ are the partially averaged (filtered) flow variables. The partially averaged NSE are obtained by applying an implicit or explicit arbitrary filter on Eqs. 2.1 and 2.2 that is constant preserving and commutes with both spatial and temporal differentiation, as is required by any filter to fulfill the averaging invariance [50]. The partial filtering is denoted by the angular brackets $\langle.\rangle$. In order to understand where the uniqueness of PANS lies, it is important to note that the filtered variables are of fundamentally different nature than the mean valued variables in RANS as well as the filtered variables in LES. The filtered PANS variables are stochastic variables as in LES, but the mean valued variables in RANS are not. However, the filtering in PANS is both spatial and temporal and arbitrary, whereas in LES it is only spatial and definite. $\tau(u_i,u_j)=\langle u_iu_j\rangle-\langle u_i\rangle\langle u_j\rangle$ is the subfilter scale (SFS) stress which is closed by modelling its anisotropic part using the eddy-viscosity (Boussinesq) assumption (Eq. 2.16).

In the above equations, $k_u=\frac{1}{2}\tau(u_i,u_i)$ is the unresolved (subfilter) kinetic energy.

The assumption in Eq. 2.16 is that the SFS-stress due to the unresolved scales are proportional to resolved rate-of-strain tensor, $\bar{S}_{ij} = \frac{1}{2}(\frac{\partial \bar{u}_i}{\partial x_j} + \frac{\partial \bar{u}_j}{x_i})$ and by the eddy viscosity of the unresolved motion ν_u. By choosing a spatial grid filter and letting $\nu_u = \nu_{sgs}$, the model described so far by Eqs. 2.14, will be an LES approach. By letting the filtering be over all spatial and temporal scales of motion, the partially filtered velocities will in fact become the mean valued velocities (RANS), the SFS stresses will become the Reynolds stresses and ν_u will become the turbulent viscosity ν_T associated with RANS. If ν_u is set to zero then Eq. 2.14 will obviously yield a DNS solution if the employed grid is fine enough to permit resolving all the scales in the flow including the dissipative scales.

In the present work, the PANS methodology based on a four equations RANS model is used (PANS $\zeta - f$). This method was derived by Basara et al. [57], [58] in order to improve the inherent faulty modelling of the near wall physics by the parent RANS in the original PANS $k - \epsilon$ model. The four equation RANS model used is the elliptic-relaxation eddy-viscosity model $k - \epsilon - \zeta - f$ proposed in [56]. In the present work the eddy viscosity of the unresolved motion is modelled as:

$$\nu_u = C_\mu \zeta_u \frac{k_u^2}{\epsilon_u} \tag{2.17}$$

Where $\zeta_u = \overline{v_u^2}/k_u$ is the velocity scale ratio of the unresolved velocity scales $\overline{v_u^2}$ and k_u. $\overline{v_u^2}$ refers to the normal fluctuating component of the velocity field to any no-slip boundary. See Durbin [55] for further details and argumentation for the concept of introducing the normal velocity scale. In the RANS $k - \epsilon - \zeta - f$ model of [56], four model equations are solved in addition to the flow equations, one equation for each model variable respectively. The corresponding PANS model equations for the unresolved variables $k_u, \epsilon_u, \zeta_u, f_u$ takes the form presented in the coming paragraphs. For details and a full motivation on all the steps on how the model equations are derived, follow the formal derivation of the PANS $k - \epsilon$ equations in [47] first and then the derivation of the PANS $\zeta - f$ equations in [57, 58].

$$\frac{\partial k_u}{\partial t} + \bar{u}_j \frac{\partial k_u}{\partial x_j} = (P_u - \epsilon_u) + \frac{\partial}{\partial x_j}[(\nu + \frac{\nu_u}{\sigma_{ku}})\frac{\partial k_u}{\partial x_j}] \tag{2.18}$$

The equation above is the model transport equation for the unresolved kinetic energy. It is derived from the exact transport equation for the SFS stress, $\tau(u_i, u_j)$, Eq. 2.13. In Eq. 2.18, $P_u = -\tau(u_i, u_j)\frac{\partial \bar{u}_i}{\partial x_j}$ is the production of the unresolved kinetic energy. This term is closed by using the constituitive relationship in Eq. 2.16. The PANS model equation for the unresolved dissipation takes the form:

$$\frac{\partial \epsilon_u}{\partial t} + \bar{u}_j \frac{\partial \epsilon_u}{\partial x_j} = C_{\epsilon 1} P_u \frac{\epsilon_u}{k_u} - C^*_{\epsilon 2} \frac{\epsilon_u^2}{k_u} + \frac{\partial}{\partial x_j}(\frac{\nu_u}{\sigma_{\epsilon_u}} \frac{\partial \epsilon_u}{\partial x_j}) \tag{2.19}$$

$$C^*_{\epsilon 2} = C_{\epsilon 1} + \frac{f_k}{f_\epsilon}(C_{\epsilon 2} - C_{\epsilon 1}); \quad \sigma_{ku,\epsilon u} = \sigma_{k,\epsilon}\frac{f_k^2}{f_\epsilon}; \quad C_{\epsilon 1} = 1.4(1 + 0.045/\sqrt{\zeta_u}) \tag{2.20}$$

The PANS model equation for ϵ_u is developed from it's RANS counterpart [47]. Here, $\sigma_{k,\epsilon}$ are the turbulent transport Prandtl numbers known from RANS. $\sigma_{ku,\epsilon u}$ are the counterparts for the unresolved kinetic energy and dissipation, respectively. As was noted in [54], the parameters f_k and f_ϵ change the value of the turbulent transport Prandtl numbers and thus modifies the turbulent diffusion terms in the equations for k_u and ϵ_u. It was also found in [54] that this change of $\sigma_{ku,\epsilon u}$ by the unresolved-to-total kinetic energy and dissipation parameters contributes to the decrease of the unresolved eddy viscosity ν_u. The PANS model equation for the unresolved velocity scale ratio ζ_u turns into:

$$\frac{\partial \zeta_u}{\partial t} + \bar{u}_j \frac{\partial \zeta_u}{\partial x_j} = f_u - \frac{\zeta_u}{k_u} P_u + \frac{\zeta_u}{k_u} \epsilon_u (1 - f_k) + \frac{\partial}{\partial x_j} \left(\frac{\nu_u}{\sigma_{\zeta u}} \frac{\partial \zeta_u}{\partial x_j} \right) \tag{2.21}$$

For the details on how the equation above was constructed, see [57, 58]. In doing so, it was however assumed that $f_\epsilon = \epsilon_u / \epsilon = 1$, i.e. that all the unresolved dissipation is in fact the RANS dissipation. This assumption is motivated by the fact that the small dissipative scales are unlikely to be resolved, since that would require a spatial resolution of the computational grid beyond the inertial subrange, i.e. DNS like resolution. It was also noted in [63] that the range of the resolved scales decreased with decreasing f_ϵ. The variable f_u in Eq. 2.21 is the elliptic relaxation function for the unresolved velocity scales ration ζ_u analogous to its RANS counterpart. The PANS Poisson equation for f_u is: [56, 57, 58].

$$L_u^2 \nabla^2 f_u - f_u = \frac{1}{T_u} (c_1 + c_2 \frac{P_u}{\epsilon_u})(\zeta_u - \frac{2}{3}) \tag{2.22}$$

The integral length and times scales L_u and T_u are computed using the unresolved kinetic energy. What is missing now is how the crucial parameter f_k is choosen. This will be explained in short. First, a summary of all the values for the constants in the equations are shown:

$$C_\mu = 0.22;\ C_{\epsilon 2} = 1.9;\ c_1 = 0.4;\ c_2 = 0.65;\ \sigma_k = 1;\ \sigma_\epsilon = 1.3;\ \sigma_{\zeta_u} = 1.2 \tag{2.23}$$

If the value of ratio of the unresolved to total kinetic energy is choosen to unity, i.e. $f_k = \frac{k_u}{k} = 1$, then the equations above collapse to the RANS equations. In the early work with PANS $k - \epsilon$ [47, 49, 51, 52], f_k was choosen as a fixed value constant in time and space during the entire simulation. As the influence of f_k on the resolved flow physics became clearer, a further step was taken in [64]. It was argued that the smallest value of f_k that a grid can support at any given location with instantaneous flow is given by:

$$f_k(\mathbf{x}, t) = \frac{1}{\sqrt{C_\mu}} \left(\frac{\Delta}{\Lambda} \right)^{2/3} \tag{2.24}$$

Where Δ is the geometric-average grid cell dimension, thus $\Delta = (\Delta x \cdot \Delta y \cdot \Delta z)^{1/3}$ and Λ is the Taylor scale of turbulence. In [65] f_k was implemented by the expression given in Eq. 2.24 as a dynamical parameter. The Taylor scale of turbulence Λ is computed using the resolved and unresolved kinetic energy and dissipation, $\Lambda = (k_u + k_{res})^{1.5} / \epsilon$. This is how it is done in the present work. f_k is computed at every location at the end of each

timestep. The values are then used as fixed values during the next timestep. Thus, Eqs. 2.14, 2.16, 2.17, 2.18, 2.19, 2.21, 2.22 and 2.24 make up the PANS $\zeta - f$ model used in the present work.

2.3 Computational Fluid Dynamics

In this work numerical simulations of the flow around various ground vehicles have been performed and analysed. The branch of fluid dynamics dealing with the numerical methods of solving the governing flow equations is known as Computational Fluid Dynamics (CFD). In order to perform an simulation of the flow, the governing equations (in this thesis the incompressible NSE, Eqs. 2.1 and 2.2) must be discretized. There exists several methods to accomplish this, including: finite differences, spectral, finite elements and finite volumes being the most common. The discretization includes several steps where numerical schemes and interpolation methods must be choosen. In this work, the CFD simulations have been carried using the commercial finite-volume based CFD software AVL Fire [66]. Equations 2.1 and 2.2 are discretized by the solver using a collocated grid arrangement. For all simulations in this work, the time-marching is done using the implicit second-order accurate three-time level scheme:

$$\left(\frac{d\phi}{dt}\right)_n = \frac{3\phi^n - 4\phi^{n-1} + \phi^{n-2}}{2\Delta t_n} \ , \ \Delta t_n = t - t_{n-1} = t_{n-1} - t_{n-2}. \tag{2.25}$$

In the cases where LES simulations have been done, the convective terms in the momentum equations have been discretized using a blend between 95% central differences (CDS) and 5% upwinding of first order accurancy. The upwinding is needed to dampen numerical occillations caused by the CDS and local insufficient grid resolution. It's generally hard to accomplish 100% CDS for complex flow cases. In the case where PANS has been used, the convective term has been discretized by using a second order upwinding scheme.

3 Summary of appended papers

3.1 Paper A

J. Östh and S. Krajnović. The flow around a simplified tractor-trailer model studied by Large Eddy Simulation. *Journal of Wind Engineering and Industrial Aerodynamics* 102 (2012), 36–47

This first paper of the thesis considers aerodynamics of heavy vehicles. Large-eddy simulation (LES) is used to study the flow around a simplified tractor-trailer model. The model consists of two boxes placed in tandem. The front box represents the cab of a tractor-trailer road vehicle and the rear box represents the trailer. The LES was made at the Reynolds number of 0.51×10^6 based on the height of the rear box and the inlet air

velocity. Two variants of the model were studied, one where the leading edges on the front box are sharp and one where the edges are rounded. One small and one large gap width between the two boxes were studied for both variants. Two computational grids were used in the LES simulations and a comparison was made with available experimental force measurements. The results of the LES simulations were used to analyze the flow field around the cab and in the gap between the two boxes of the tractor-trailer model. Large vortical structures around the front box and in the gap were identified. The flow field analysis showed how these large vortical structures are responsible for the difference in the drag force for the model that arises when the leading edges on the front box are rounded and the gap width is varied. Some of this work has been published in the attended related publication I.

3.2 Paper B

S. Krajnović and J. Östh. LES Study of breakdown control of A-pillar vortex. *Int. J. Flow control* 2.4 (2010), 237–257

In this paper, a passenger vehicle flow is considered. A longitudinal vortex, called the A-pillar vortex, is formed along the side wind screens of passenger cars. This vortex is responsible for induced drag on the vehicle due to the momentum transferred from the moving vehicle to the air entrapped in the vortex. It is also the main contributor to in-cabin noise for the passenger inside the vehicle as well as dirt and water distribution on the side of the car. These kinds of longitudinal vortices are in themself extremely complex flow phenomenons. Their most familiar occurence is maybe on the suction side on the delta wing. They undergo a phenomen called "vortex breakdown", which is characterized by a sudden decrease in the axial flow and stagnation of the flow inside the core, as well as rapid increase in the pressure inside the core and a decrease in the tangential velocity. In this paper, active flow control of the longitudinal vortices were studied using LES. The LES results were validated against existing Particle Image Velocitimetry (PIV) and aerodynamic drag data. The LES results were further used to study the flow physics responsible for the development of the longitudinal vortex, in particular the vortex breakdown process. Tangential blowing and suction into the separating shear layer forming the longitudinal vortex was found to be a sensitive process that can cause instabilities in the flow. The resulting LES flows also show that actuation influences not only the longitudinal vortex nearest to the actuation slot but also the overall flow. Thus, the influence of the flow control acuation on the entire flow must be considered in order to be able to find the apporpriate level of control for optimal aerodynamic performance.

3.3 Paper C

J. Östh and S. Krajnović. A study of the aerodynamics of a generic freight wagon with a container using Large Eddy Simulation. *Journal of Fluids and Structures* (2012), Under

consideration

The focus of the work in this paper is entirely dedicated to the physics of the unsteady flow around a container freight wagon. Therefore, the well-known and established method of LES with the Standard Smagorinsky model was used as in the previous papers. The generic container freight wagon model consists of one 11.8 m standard container placed on a wagon. Details on the undercarriage such as wheels are included, but the model is generic and smoothed in comparison to a real freight wagon. This model has not been investigated experimentally in wind tunnel by us or any other researchers previously. Therefore, a fairly low Reynolds number was choosen and two grids which both provided excellent spatial resolution were constructed in order to get reliable results. An examination of the flow close to the surface on the container's roof revealed that even low and high speed streaks were resolved in a plane located 5 viscous units from the wall. The choosen Reynolds number of the flow was 10^5 based on the width of the container. A previous experimental study [67] of the flow around one double-stacked container freight wagon has shown that the drag coefficient obtains self similarity for Reynolds numbers above approximately $0.8 \cdot 10^5$. The results recorded from the simulations were used to analyse and describe both the mean and the instantaneous flow around the wagon. The flow around the front was found to be dominated by regions of massive separated flow. The flow beneath the wagon was found to be irregular and chaotic. Some of this work has been published in the attended related publication II.

3.4 Paper D

J. Östh and S. Krajnović. "Simulations of flow around a simplified train model with a drag reducing device using Partially Averaged Navier-Stokes". *Conference on Modelling Fluid Flow (CMFF'12), The 15th International Conference on Fluid Flow Technologies.* Budapest, Hungary, 4-7 September, 2012

This paper examines the flow around a regional train model with similar rectangular geometrical features as the Bombardier Contessa train which is used in Sweden. The train model has previously been studied in wind tunnel experiments [68] and has a length to height/width ratio of 7:1. The Reynolds number based on the height of the train model is $0.37 \cdot 10^6$. For this Reynolds number, the flow separates from the curved leading edges on the front then attaches again on the roof and sides forming a boundary layer there before separating in the wake. The high Reynolds number and the length of the train makes the flow around it a difficult task to predict. It is unfeasible to make an accurate and well resolved LES simulation of the flow around it. Therefore, the recently developed hybrid turbulence technique Partially Averaged Navier Stokes (PANS) was choosen. The objective for the research in this paper is two-fold. The first objective is to evaluate PANS for this kind of vehicle aerodynamic flows and the second objective is to decrease the drag on the train model by some add-on device. The add-on device that was choosen was an open cavity placed at the base of the train model. Even though this

might not be the most practically construction for a real train, the device was choosen in order to get a starting point for further investigations later on. Two cases of the flow around the train model were simulated in the paper. The first case is of the natural flow around the train model where direct comparison to experimental data of drag coefficient and pressure coefficient are made. In the second case an open cavity is placed on the base of the train model with the aim of reducing the overall drag on the model. The results show that the drag for model with the cavity is reduced by some 10% compared to the drag of the natural case. The agreement to experimental data for the natural case is not perfect but the general features in the flow field are simulated correctly.

4 Conclusions and future work

4.1 Conclusions

The work so far includes simulations and analyses of the flows around four different vehicle models. In the first paper, the complex flow around a simplified tractor-trailer model was simulated and particular efforts was put into the analyses of the flow around the tractor and in the gap. It was seen how small geometrical changes in the design such as rounding of the front edges totally changed the flow in the gap, and thereby the overall drag coefficient. It was found that it was in particular the vortices formed on the outside of the tractor that was mainly responsible for the large discrepancies in the drag coefficient. Even though the model was a generic tractor-trailer, the same kind of gap flow situations occur in the flow around freight trains where the wagons are separated by a gap and contributes significantly to the drag coefficients of such train configurations.

The second paper address the control of the flow around a passenger car vehicle and particular the break down of the so called A-pillar vortex. The A-pillar vortex is a longitudinal vortex formed outside of the side windows of the vehicle by the flow separating from the sides of the front of the vehicle. This flow is very complex and physics of the breakdown and the vortex is indeed a intricate phenomena to study in itself. The simulations showed that by blowing air into the vortex, and thereby increase the level of vorticity in the separating shear layers, that the breakdown of the vortex was precipitated. This is interesting for the aerodynamics of trains was well, since a similar type of longitudinal vortex along the train is formed during cross winds. This vortex acts as an lever on the train and can in extreme cases overturn the train. Thus, the research presented in the second paper is relevant to train aerodynamics as well.

In the third paper the flow around one container freight wagon was explored. The main findings is the complexity of the flow underneath the wagon and that as much as 25% of the drag comes from the underhood. Since only one single-standing wagon was considered in the study, the relative contribution from the underhood to the total drag coefficient can be expected to be higher for a wagon submerged into a real freight train with wagons ahead of it and behind it, thereby reducing the contribution from the pressure difference between the front face and the rear face. This is an interesting finding

which will be addressed in future work.

The fourth and last paper presented a simulation of the flow around a model of a regional train. Since the Reynolds number was quite high, and the edges on the front of the model was rounded, this flow would demand approximately a grid consisting 100 millions cells if the flow should be resolved as accurately as in the cases in the previous papers. This is not practical for the purpose of the research within this project. Therefore the hybrid method PANS was used to simulate the flow. Using PANS, the high demand of cells required by LES could be relaxed, and the flow was simulated with some flaws in comparison to experimental data. No perfect match was obtained in the comparison with pressure data from experiments and drag coefficient, but at least the general features in the flow was simulated correctly. Especially the separation from the front edges was predicted, although the separation bubble was too large, which affects the drag coefficient immensly as well as the flow along the train. In addition to evaluating PANS for this kind of flows, a drag reducing device was also tested. The device was a cavity placed on the rear. It was shown that the drag was reduced by some 10% by this cavity. Even though the cavity might not be a realistic option for real trains, the simulation provides a starting point for future research.

4.2 Future work

4.2.1 Wind tunnel experiments on a freight train

During the fall of 2012 wind tunnel experiments will be conducted within the project in the wind tunnel at Chalmers on a generic freight train. The train is shown in Fig. 4.1 and the configuration consists of one locomotive and three consecutive container wagons of the same generic model that has been studied in Paper C. Force measurements and possibly PIV measurements will be conducted on the second wagon in order to get a better representation of a real wagon in a freight train. In the study by Watkins et al. [69] it was found that, for a wagon not to experience effects in the measured drag coefficient from the locomotive and or the end of the train, one and a half dummy wagons were needed ahead of the wagon being studied. One half dummy wagon was needed downstream. Two simple add-on devices will be put on the second wagon in order to try to reduce the drag on it, see Fig 4.2. The first device is a side skirt which will prevent air from being sucked in under the wagon. The second device will be a vertical plate placed in the gap. Measurements will be done for 0, 5 and 10 degrees of yaw angle for all configurations.

The area of the test section of the wind tunnel is 1.28m x 1.25m. The width of the full-scale train is 2.4 m and the length of the total train configuration will be 54 m. The scale of the train model is choosen to 1:25. This will give a maximum blockage in the wind tunnel at 10 degree yaw angle of 4.5%. The Reynolds number will be 100 000 which is the same as the previous LES simulation on the single container wagon. This will require a free streaming velocity of 27.5 m/s with air at room temperature as the working fluid.

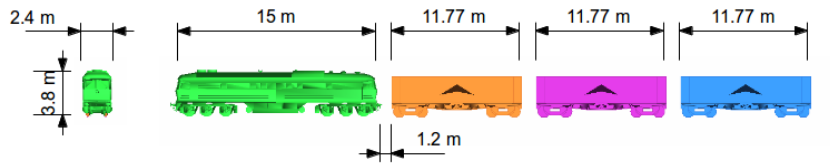

Figure 4.1: *Train configurations for upcoming wind tunnel experiments in dimensions of a real train.*

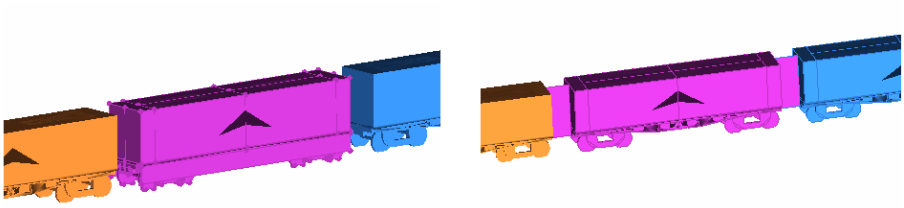

Figure 4.2: *Two simple add-on devices on the freight wagon. Left figure shows side skirts and right figure shows a vertical plate in the gap.*

4.2.2 Guiding vanes

A more practically feasible add-on device on the regional train model than the cavity that has been studied so far in Paper D is to use guiding vanes at the edges on the base of the train. Such guiding vanes has been used on a scale tractor-trailer model by Tsai [70]. The research in [70] aims at reducing the drag with guiding vanes installed at the rear end of a truck that change the wake flow. The study was performed as a wind tunnel experiment on a 1:8 scale heavy truck model at a Reynolds number of $1.8{\cdot}10^6$.

The variables of flow turning angle (Θ_1 in Fig. 4.5) and the area ratio of the nozzles were analysed to determine the effectiveness of drag reduction. The results from the experiments indicated that the highest drag reduction at low Reynolds numbers was achieved using a divergent nozzle with turning angle of 60 degrees and an inlet-to-outlet ratio of 2.5. In total 12 different configurations with different Θ_1 and inlet-to-outlet ratios were tested in [70]. The drag reduction on the truck turned out to be as much as up to 15% for the optimal configuration, while some configurations lead to an increased drag.

Guiding vanes will be evaluated on the regional train model using PANS. An open question regarding the guiding vanes is how the inlet width of the vanes in relation to the

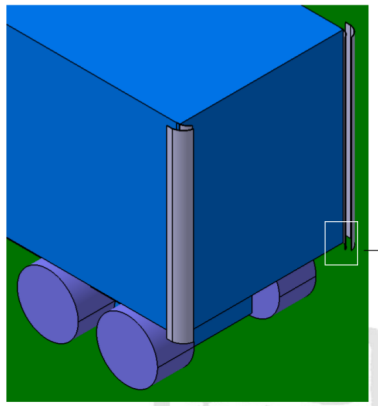

Figure 4.3: *Guiding vanes placed on the rear edges of a tractor-trailer. The figure is taken from [70].*

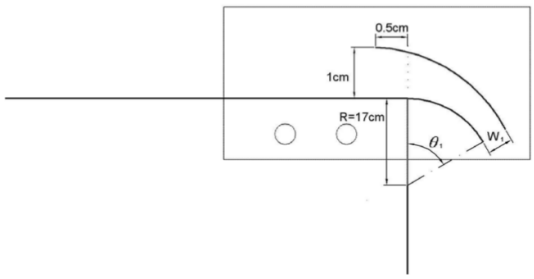

Figure 4.4: *Decisive parameters in the design of guiding vanes. The figure is taken from [70].*

approaching boundary layer thickness affects the effectivity of the guiding vanes. In the work by Tsai [70] on the tractor-trailer model, the boundary layer in front of the guiding vanes was not measured, but it was estimated from the flat boundary layer equations. This is not expected to yield an accurate estimate of the actual size at all since the flow situation on the side of the truck is different from a flat boundary layer due to the initial separation on the beginning of the trailer. Thus, what the relationship in the experimental study was of the boundary layer thickness to the inlet width of the vanes is unknown. Thus, the effect of varying the inlet width will be of interest on the regional train model. Another geometrical difference between the regional train model and the truck is that on the truck the rear edges is sharp, and thus the guiding vanes used an inner plate (see Fig. 4.5) with a radius to make inner curved edges. Since on the regional train model, the rear edges are rounded these edges will be used as the inner edges which will not have the same radius as on the truck.

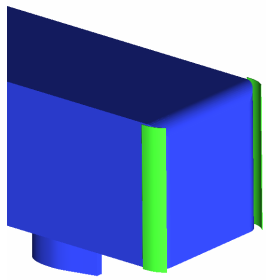

Figure 4.5: *Guiding vanes on the regional train model.*

References

[1] J. Östh and S. Krajnović. The flow around a simplified tractor-trailer model studied by Large Eddy Simulation. *Journal of Wind Engineering and Industrial Aerodynamics* 102 (2012), 36–47.

[2] S. Krajnović and J. Östh. LES Study of breakdown control of A-pillar vortex. *Int. J. Flow control* 2.4 (2010), 237–257.

[3] J. Östh and S. Krajnović. A study of the aerodynamics of a generic freight wagon with a container using Large Eddy Simulation. *Journal of Fluids and Structures* (2012), Under consideration.

[4] J. Östh and S. Krajnović. "Simulations of flow around a simplified train model with a drag reducing device using Partially Averaged Navier-Stokes". *Conference on Modelling Fluid Flow (CMFF'12), The 15th International Conference on Fluid Flow Technologies*. Budapest, Hungary, 4-7 September, 2012.

[5] J. Östh and S. Krajnović. "A LES Study of a Simplified Tractor-Trailer Model". *The Aerodynamics of Heavy Vehicles III: Trucks, Buses, and Trains*. Vol. 1. Potsdam, Germany, 2010.

[6] J. Östh and S. Krajnović. "Large Eddy Simulation of the Flow around one Single-Stacked Container Freight Wagon". *Proceedings of the First International Conference on Railway Technology: Research, Development and Maintenance*. Ed. by J. Pombo. Civil-Comp Press, Stirlingshire, Scotland, paper 162, 2012.

[7] G. I. Figura-Hardy. 2007 RSSB Slipstream Safety - Analysis of existing experimental data on train slipstreams including the effects on pushchairs. *Rail Safety and Standards Board* (2007).

[8] M. Sterling, C. J. Baker, S. C. Jordan, and T. Johnson. A study of the slipstreams of high-speed passenger trains and freight trains. *Proc. IMechE, Part F: Journal of Rail and Rapid Transit* 222 (2008), 177–193.

[9] T. W. Muld. "Slipstream and Flow Structures in the Near Wake of High-Speed Trains". ISBN/ISSN 978-91-7501-392-3. PhD thesis. Stockholm, Sweden: Royal Institute of Technology, 2012.

[10] H. Hemida, N. Gil, and C. Baker. LES Study of the slipstream of a rotating train. *ASME: Journal of Fluids Engineering* 132 (2010),

[11] H. Hemida. "Numerical Simulations of Flows around Trains and Buses in Cross Winds". ISBN/ISSN 978-91-7385-187-9. PhD thesis. Gothenburg, Sweden: Chalmers University of Technology, 2008.

[12] S. Krajnović, P. Ringqvist, and B. Basara. "Large Eddy Simulation of the flow around a simplified train moving through a crosswind flow". *Proceedings of the First International Conference on Railway Technology: Research, Development and Maintenance*. Ed. by J. Pombo. Civil-Comp Press, Stirlingshire, Scotland, paper 153, 2012.

[13] H. Kim. Aerodynamic analysis of a train running in a tunnel. *Korean Soc. Mech. Eng. (KSME)* 21(8) (1997), 963–72.

[14] H. Kim. Aerodynamic drag on trains in tunnels. 1. Synthesis and definitions. *Proc. World Congr. Inst. Mech. Eng.* 210 (1996), 29–38.

[15] H. Kim. Aerodynamic drag on trains in tunnels. 2. Prediction and validation. *Proc. World Congr. Inst. Mech. Eng.* 210 (1996), 39–49.

[16] R. S. Raghunathan, H.-D. Kim, and T. Setoguchi. Aerodynamics of high-speed railway train. *Progress in Aerospace Sciences* 38 (2002), 469–514.

[17] D. Heine and K. Ehrenfried. "Experimental Study of the Compression-Wave Generation due to Train-Tunnel Entry". *Proceedings of the First International Conference on Railway Technology: Research, Development and Maintenance*. Ed. by J. Pombo. Civil-Comp Press, Stirlingshire, Scotland, paper 163, 2012.

[18] D. Uystepruyst, W.-L. Mame, E. Creuśe, and S. Nicaise. Efficient 3D numerical prediction of the pressure wave generated by high-speed trains entering tunnels. *Computers & Fluids* 47 (2011), 165–177.

[19] M. Jönsson, C. Wagner, and S. Loose. "High-speed particle image velocimetry of the underfloor flow of a generic high-speed train model". *Proceedings of the First International Conference on Railway Technology: Research, Development and Maintenance*. Ed. by J. Pombo. Civil-Comp Press, Stirlingshire, Scotland, paper 153, 2012.

[20] W. King III. A précis of developments in the aeroacoustics of fast trains. *Journal of Sound and Vibration* 193.1 (1996), 349 –358.

[21] W. J. Davis. The tractive resistance of electric locomotives and cars. *Gen. Electr. Rev.* 29 (1926), 2–24.

[22] B. P. Rochard and F. Schmid. A review of methods to measure and calculate train resistances. *Proc. IMechE, Part F: Journal of Rail and Rapid Transit* 214 (2000), 185–199.

[23] P. Lukaszewicz. Running resistance - results and analysis of full-scale tests with passenger and freight trains in Sweden. *Proc. IMechE, Part F: Journal of Rail and Rapid Transit* 221 (2006), 183–193.

[24] P. Lukaszewicz. "Energy Consumption and Running Time for Trains". PhD thesis. Royal Institute of Technology, 2001.

[25] R. Engdahl. "Full-scale rail car testing to determine the effect of position-in-train on aerodynamic resistance". *Publication R-705*. Association of American Railroads, 1987.

[26] R. Engdahl, G. R.L., and J. C. Paul. “Train resistance - aerodynamics Volume II, Open top car application”. *Proc., Railroad Energy Technology Conference II*. Atlanta, GA.: Association of American Railroads, 1986, pp. 225–242.

[27] S. Hoerner. “Efficiency of Railroad Trains”. *Fluid Dynamic Drag*. Hoerner Fluid Dynamics, Brick Town, New Jersey, 1965,

[28] Johansen. Air Resistance of Trains. *Proc. Institute Mech. Engineers* 134 (1936), p.91.

[29] A. Orellano and S. Sperling. “Aerodynamic Improvements and Associated Energy Demand Reduction of Trains”. *The Aerodynamics of Heavy Vehicles II: Trucks, Buses, and Trains*. Vol. 41. Springer Berlin / Heidelberg, 2009, pp. 219–231.

[30] W.-H. Hucho. *Aerodynamics of Road Vehicles*. 4th ed. ISBN 0-7680-0029-7. Society of Automotive Engineers, Inc., 1998.

[31] K. R. Cooper. “Truck Aerodynamics Reborn - Lessons from the Past”. SAE Paper 2003-01-3376, 2003.

[32] K. R. Cooper. “Commercial Vehicle Aerodynamic Drag Reduction: Historical Perspective as a Guide”. *The Aerodynamics of Heavy Vehicles: Trucks, Busses and Trains*. Monterey, USA, 2002.

[33] R. M. Wood and S. X. S. Bauer. “Simple and Low-cost aerodynamic drag reduction devices for a tractor-trailer”. SAE Paper 2003-01-3377, 2003.

[34] El-Alti, Mohammad, Chernoray, Valery, Jahanmiri, Mohsen, and Davidson, Lars. Experimental and computational studies of active flow control on a model truck-trailer. *EPJ Web of Conferences* 25 (2012), 01012. DOI: 10.1051/epjconf/20122501012.

[35] B. Khalighi et al. “Experimental and computational study of unsteady flow behind a Bluff Body with a drag reduction device”. SAE Paper 2001-01-1042, 2001.

[36] R. Verzicco, M. Fatica, G. Laccarino, and P. Moin. Large Eddy Simulation of a road vehicle with drag-reduction devices. *AIAA Journal* 40 (2002), 2447–2455.

[37] J. D. Coon and K. Visser. “Drag Reduction of a Tractor-Trailer Using Planar Boat Tail Plates”. *The Aerodynamics of Heavy Vehicles: Trucks, Buses, and Trains*. Vol. 1. Springer Berlin / Heidelberg, 2004. ISBN: 3-540-22088-7.

[38] C. R. Doering. The 3D Navier-Stokes Problem. *Ann. Rev. Fluid Mech.* 41 (2009), 109–128.

[39] S. B. Pope. *Turbulent Flows*. first edition. Cambridge: Cambridge University Press, 2000.

[40] P. Sagaut. *Large Eddy Simulation for Incompressible Flows*. Third ed. Springer, 2006. ISBN: 3-540-26344-6.

[41] J. Smagorinsky. General circulation experiments with the primitive equations. *Monthly Weather Review* 91.3 (1963), 99–165.

[42] S. Krajnović. “Large-Eddy Simulation for Computing the Flow Around Vehicles”. ISBN/ISSN 91-7291-188-3. PhD thesis. Gothenburg, Sweden: Chalmers University of Technology, 2002.

[43] S. Krajnović. LES of Flows Around Ground Vehicles and Other Bluff Bodies. *Philosophical Transactions of the Royal Society A* 367.1899 (2009), 2917–2930.

[44] E. Wassen and F. Thiele. Road Vehicle Drag Reduction by Combined Steady Blowing and Suction. *AIAA Paper 2009-4174*. (2009).

[45] S. Ghosal and P. Moin. The Basic Equations for the Large Eddy Simulation of Turbulent Flows in Complex Geometry. *Journal of Computational Physics* 118 (1995), 24–37.

[46] J.-L. Guermond, J. T. Oden, and S. Prudhomme. Mathematical Perspectives on Large Eddy Simulation Models for Turbulent Flows. *Journal of Mathematical Fluid Mechanics* 6 (2 2004), 194–248.

[47] S. S. Girimaji. Partially-Averaged Navier-Stokes Model for Turbulence: A Reynolds-Averaged Navier-Stokes to Direct Numerical Simulation Bridging Method. *Journal of Applied Mechanics* 73 (2006), 413–421.

[48] M. R. Khorrami, B. SInger, and M. E. Berkman. Time-accurate simulations and acoustic analysis of slat free shear layer. *AIAA Journal* 40 (2002), 1284–1291.

[49] S. S. Girimaji, E. Jeong, and R. Srinivasan. Partially-Averaged Navier-Stokes Method for Turbulence: Fixed Point Analysis and Comparison With Unsteady Averaged Navier-Stokes. *Journal of Applied Mechanics* 73 (2006), 422–428.

[50] M. Germano. Turbulence: the filtering approach. *Journal of Fluid Mechanics* 238 (1992), 325–336.

[51] E. Jeong and S. S. Girimaji. Partially-Averaged Navier-Stokes Method for Turbulence Simulations - Flow Past a Square Cylinder. *ASME: Journal of Fluids Engineering* 132 (2010),

[52] S. Lakshmipathy and S. S. Girimaji. Partially-Averaged Navier-Stokes Method for Turbulence Simulations - Flow Past a Circular Cylinder. *ASME: Journal of Fluids Engineering* 73 (2010),

[53] S. Lakshmipathy and S. S. Girimaji. Partially-Averaged Navier-Stokes Method for Turbulent Flows - $k - \omega$ implementation. (2006), AIAA Paper 2006–119.

[54] J. Ma, S. Peng, L. Davidson, and F. Wang. A Low Reynolds Number Variant of Partially-Averaged Navier-Stokes Model for Turbulence. *Int. J. Heat and Fluid Flow* 2011 (2011), 652–669.

[55] P. A. Durbin. Near-Wall Turbulence Closure Modeling Without Damping Functions. *Theoretical and Computational Fluid Dynamics* 3 (1991), 1–13.

[56] K. Hanjalić, M. Popovac, and Hadžiabdić. A robust near-wall elliptic-relaxation eddy-viscosity turbulence model for CFD. *Int. J. Heat and Fluid Flow* 25 (2004), 1047–1051.

[57] B. Basara, S. Krajnović, and S. S. Girimaji. PANS methodology applied to elliptic relaxation-based eddy viscosity transport model. *Proceedings of Turbulence and Interactions* (2009),

[58] B. Basara, S. Krajnović, S. S. Girimaji, and Z. Pavlovic. Partially Averaged Navier-Stokes Method for Turbulence Simulations: Near-Wall Eddy Viscosity Transport Model Implementation. *AIAA Journal* 49 (12) (2011), s. 2627–2636.

[59] S. Krajnović. Flow around a tall finite cylinder explored by large eddy simulation. *Journal of Fluid Mechanics* 676 (2011), 294–317.

[60] S. Krajnović, R. Lárusson, E. Helgason, and B. Basara. PANS of Rudimentary Landing Gear. *AIAA Paper AIAA-2011-3109. Nr. 153761* (2011).

[61] Proceedings (CDROM) of the AIAA-NASA workshop on benchmark problems for airframe noise computations-I (BANC-I) (June 9-11, 2010).

[62] P. R. Spalart and K. M. Mejia. Analysis of Experimental and Numerical Studies of the Rudimentary Landing Gear (2011), AIAA paper 2011–0355.

[63] A. Frendi, A. Tosh, and S. S. Girimaji. Flow past a backward-facing step: Comparison of PANS, DES and URANS results with experiments. *International journal for Computational Methods in Engineering Science and Mechanics* 8 (2007), 23–38.

[64] S. S. Girimaji and K. S. Abdol-Hamid. "Partially-Averaged Navier-Stokes for Turbulence: Implementation and Validation". *43rd AIAA Aerospace Science Meeting and Exhibit*. Reno, Nevada, AIAA-paper 2005-0502, 2005.

[65] B. Basara, S. Krajnović, and S. S. Girimaji. "PANS VS. LES for computations of the flow around a 3D bluff body". *7th International ERCOFTAC Symposium on "Engineering Turbulence Modelling and Measurements*. Limassol, Cyprus., 2008.

[66] AVL. CFD Solver. AVL Fire Manual, v2010.1, edition 11/2010. 2010.

[67] F. Alam and S. Watkins. "Lateral stability of a double stacked container wagon under crosswinds". *Proceedings of the International Conference on Mechanical Engineering 2007 (ICME2007)*. Dhaka, Bangladesh, 2007, pp. 225–242.

[68] Y. Sakuma and A. Ido. Wind Tunnel Experiments on Reducing Separated Flow Region Around Front Ends of Vehicles on Meter-Gauge Railway Lines. *Quarterly Report of RTRI* 50.1 (2009), 20–25.

[69] S. Watkins, J. Saunders, and H. Kumar. Aerodynamic drag reduction of goods trains. *Journal of Wind Engineering and Industrial Aerodynamics* 40 (1992), 147–178.

[70] M. Tsai. "The Study of using corner nozzle flow for truck drag reduction". MA thesis. Tainan City, Taiwan: National Cheng Kung University, 2009.